Artificial Intelligence and Machine Learning Review
Scipublication
DOI: 10.69987/AIMLR.2024.50309

AI-Driven Procedural Animation Generation for Personalized Medical Training via Diffusion-Based Motion Synthesis

Zan Li[1], *Zi Wang*[1.2]
[1] *School of Journalism and Communication, Peking University, Beijing, China*
[1.2] *Animation and Digital Arts, University of Southern California, CA, USA*

Keywords

Medical Training,
Diffusion Models,
Procedural Animation,
Adaptive Learning

Abstract

Medical education faces critical challenges in providing standardized, accessible, and personalized training content. Traditional manual animation creation requires extensive resources and time, limiting scalability. This paper presents an end-to-end framework that automatically generates high-quality, personalized medical training animations from clinical guidelines using diffusion-based motion synthesis. Our approach integrates natural language processing for medical concept extraction, knowledge graph construction for procedural representation, and a domain-adapted diffusion model with anatomical constraints. We introduce complexity-aware adaptive rendering techniques derived from game engine optimization to achieve real-time performance. Real-time cognitive load monitoring enables dynamic content adaptation. Comprehensive evaluation with 120 medical students demonstrates 23% improvement in learning outcomes and 35% reduction in training time. The system achieves 92 FPS on RTX 3070 and 72 FPS on Quest 2 while maintaining medical accuracy validated by board-certified surgeons (mean rating 4.6/5.0).

1. Introduction

1.1 Motivation and Clinical Challenges in Medical Training

Contemporary medical education confronts substantial barriers in delivering effective procedural training. The global shortage of qualified surgical instructors constrains training capacity, particularly affecting resource-limited regions. Traditional apprenticeship models expose patients to potential risks during trainee learning curves. some studies suggest medical errors could be among the leading causes of death; however, estimates vary and remain debated in healthcare systems, with inadequate training contributing significantly to adverse events. Comprehensive simulation training can reduce surgical errors by up to 50% and decrease operation time by 29%. Virtual reality surgical simulators established foundational architectures for haptic-enabled arthroscopic surgery simulation, demonstrating feasibility of real-time soft tissue deformation using finite element analysis[1]. Yet content creation remains a bottleneck. Developing a single high-fidelity medical animation typically requires 3-6 months and costs between $50,000-$200,000. The heterogeneity of learner populations presents additional challenges, with trainees spanning diverse experience levels requiring tailored content depth and pacing. Deep learning approaches have automated continuous performance monitoring during Virtual Reality (VR) simulation[2].

1.2 Limitations of Existing Medical Animation Approaches

Existing medical training animation methodologies exhibit several critical limitations. Manual 3D animation production workflows demand specialized expertise in both medical domains and computer graphics. Commercial virtual reality platforms offer limited content libraries, with new procedure development cycles extending 6-12 months. Template-based procedural generation methods require extensive programming knowledge, restricting content creation to technical specialists. Recent generative AI approaches show potential but lack medical domain specialization. In medical imaging, diffusion models have demonstrated superior performance for synthesizing high-quality 3D CT and MRI data, yet general-purpose models frequently generate anatomically implausible results in medical contexts[3]. Real-time rendering optimization has not fully leveraged game engine technologies. Neural surface reconstruction techniques like EndoSurf enable real-time rendering of deformable surgical scenarios[4]. Generative AI for transformative healthcare has been comprehensively studied, revealing both substantial potential and current limitations[5].

1.3 Our Approach and Key Contributions

This paper introduces a comprehensive framework addressing these limitations through four integrated innovations. First, we develop an automated pipeline transforming unstructured clinical guideline text into executable animation specifications via natural language processing and medical knowledge graph construction. Generative AI-based virtual assistants in immersive VR environments demonstrate potential for anatomy education enhancement[6]. Second, we propose a medical motion diffusion model incorporating anatomical constraints and expert feedback. Third, we present complexity-aware adaptive rendering algorithms dynamically adjusting geometric and temporal detail, achieving 90+ FPS on consumer VR hardware. The influence of generative AI on healthcare industries enhanced by the metaverse provides important context[7]. Fourth, we implement real-time cognitive load monitoring using physiological signals to drive personalized content adaptation. Synthetic patients can simulate difficult conversations with multimodal generative AI[8]. Multi-layer Gaussian splatting techniques enable immersive anatomy visualization[9]. Controlled experiments with 120 medical students demonstrate statistically significant improvements.

2. Related Work

2.1 Medical Training Simulation and VR-Based Education

2.1.1 Virtual Reality Surgical Training Systems

Virtual reality has emerged as a transformative modality for surgical skills acquisition. Contemporary platforms have validated clinical effectiveness, with VR-trained surgeons completing procedures 29% faster and committing 50% fewer errors. Commercial systems like PrecisionOS and Osso VR employ Unity or Unreal Engine for physics simulation and rendering. Content production remains predominantly manual, with specialized teams creating procedure-specific modules through months-long development cycles. Motion-guided video generation approaches have been applied to laparoscopic surgery, producing temporally coherent surgical video sequences[10]. Advanced 3D medical diffusion architectures achieve controllable high-resolution volumetric synthesis through patch-volume autoencoders[11].

2.1.2 Medical Procedure Visualization and Education

Three-dimensional medical animation has evolved from static anatomical models to interactive procedural demonstrations. Educational research confirms that 3D visualizations significantly enhance spatial comprehension and information retention compared to traditional 2D textbook illustrations. Production of medical animations traditionally involves medical illustrators collaborating with subject matter experts to create accurate visual representations. This labor-intensive process yields high-quality content but scales poorly to comprehensive medical curricula. Generative AI applications are enhancing medical training through automated content generation and personalized learning experiences[12].

2.1.3 Skill Assessment and Adaptive Learning

Competency-based medical education emphasizes objective skill assessment through validated metrics. Frameworks such as Objective Structured Assessment of Technical Skills (OSATS) provide standardized rubrics for evaluating surgical proficiency. Adaptive learning systems personalize educational experiences by adjusting content difficulty and pacing. Implementation in medical education shows promise, with adaptive platforms demonstrating 18% higher pass rates. Teaching medicine with generative artificial intelligence reveals practices, pitfalls, and possibilities that inform effective implementation[13]. Cognitive load theory provides theoretical foundations for understanding how instructional design affects learning efficiency.

2.2 Generative AI for Medical Animation

Denoising diffusion probabilistic models have revolutionized generative modeling across multiple domains. Motion diffusion models extend these principles to human motion synthesis, conditioning generation on textual descriptions or spatial constraints. Generative AI for biomedical video synthesis has been comprehensively reviewed, highlighting advances in motion generation and temporal consistency[14]. Large language models exhibit remarkable capabilities in understanding and generating structured information from natural language text. Medical NLP systems extract clinical concepts from unstructured documentation, identifying entities such as anatomical structures, procedures, and diagnoses. Knowledge graph construction leverages these extraction capabilities to represent complex procedural knowledge. A synergistic fusion of AI and VR elevates medical training through immersive anatomy learning and practical procedure mastery[15].

2.3 Real-Time Rendering and Optimization

Level-of-detail algorithms dynamically adjust geometric complexity to balance visual quality and computational performance. Discrete LOD approaches precompute multiple resolution variants of objects, selecting appropriate versions based on viewing distance. Scene complexity assessment guides dynamic rendering quality adjustment to maintain target frame rates. Advanced techniques such as foveated rendering exploit eye-tracking data to allocate rendering resources to gaze locations. Medical simulation demands particularly stringent performance requirements due to real-time interaction and stereoscopic rendering overhead. Game engines including Unreal Engine and Unity have been adapted for medical applications, achieving unprecedented real-time performance for complex surgical scenarios.

3. Methodology

3.1 System Overview and Pipeline Architecture

Our framework comprises four interconnected modules processing clinical guidelines into personalized training animations. The Clinical Guideline Processing module ingests PDF documents and textual protocols, applying NLP to extract medical entities and relationships. Extracted information populates a procedural knowledge graph encoding surgical steps, anatomical structures, instrument requirements, and temporal dependencies. The Animation Specification Generator translates graph nodes and edges into executable animation parameters. The Motion Generation module implements a medical-adapted diffusion model conditioned on animation specifications and textual descriptions. Generated motion sequences undergo physics-based soft tissue simulation. The Adaptive Rendering module analyzes procedure complexity, user expertise, and real-time performance metrics to dynamically select detail levels. The Personalization Engine continuously monitors user physiological signals and interaction patterns to estimate cognitive load. Classification models operating on ECG and galvanic skin response features categorize load into discrete levels. Detected cognitive states trigger content adaptation mechanisms.

Table 1: System Module Specifications and Data Flow

Module	Input	Output	Processing Time	Key Technologies
Guideline Processing	PDF/Text (2-50 pages)	Knowledge Graph (150-500 nodes)	8-15 seconds	BioBERT, cTAKES, GPT-4
Animation Specification	Knowledge Graph + Templates	JSON Animation Config	2-3 seconds	Graph Neural Networks
Motion Generation	Specification + Text Prompt	3D Motion Sequence (frame count: 30-120)	35-50 seconds	Diffusion Model, Physics
Adaptive Rendering	Motion + User State + Scene	Rendered Frames (72-120 FPS)	Real-time (<11ms/frame)	Octree-GS, GPU Tessellation
Personalization	ECG/GSR + Interaction Logs	Adaptation Parameters	<5ms (inference)	ResNet-LSTM Classifier

3.2 Clinical Guideline Parsing and Knowledge Extraction

3.2.1 NLP-Based Medical Concept Extraction

Medical named entity recognition forms the foundation of automated guideline processing. Our pipeline employs a cascaded architecture combining rule-based preprocessing with neural sequence labeling. The cTAKES framework provides initial tokenization and entity identification using UMLS Metathesaurus. BioBERT contextual embeddings capture semantic relationships between medical terms. Conditional random field layers perform sequence tagging to identify entity boundaries and types across categories including anatomical structures, medical devices, surgical actions, and pathological states. Post-processing modules resolve abbreviation expansions and perform negation detection. We achieve entity recognition F1 scores of 0.94 on clinical guideline evaluation datasets, with term standardization accuracy of 0.91 when mapping to SNOMED CT and ICD-10 coding systems.

3.2.2 Procedural Knowledge Graph Construction

Extracted entities and relations populate a domain-specific knowledge graph schema representing surgical procedures as structured workflows. Graph nodes encode typed entities including anatomical regions with spatial coordinates, surgical instruments with physical properties, procedural steps with duration estimates, and clinical objectives. Directed edges represent relationships such as temporal precedence, spatial adjacency, and instrument requirements. Large language model prompting facilitates triple extraction from guideline text. Few-shot learning provides examples of desired entity-relation-entity tuples. Graph neural networks trained on existing medical ontologies predict missing edges through link prediction. Expert validation interfaces enable medical professionals to review and augment automatically constructed graphs. Validation sessions with 8 board-certified surgeons achieved inter-rater reliability Fleiss' kappa of 0.78.

3.2.3 Animation Specification Generation

Knowledge graph nodes and edges map systematically to animation parameters through learned transformation rules. Graph node attributes determine 3D asset selections from medical model libraries. Anatomical structure nodes reference volumetric meshes reconstructed from CT imaging. Action nodes encode motion primitives including grasping, cutting, suturing, and irrigation. Edge relationships define spatial and temporal constraints. Precedence edges establish ordering dependencies. Spatial edges specify relative positioning requirements translated into inverse kinematics target constraints. JSON schema specifications standardize animation descriptions for consumption by the motion generation module.

Figure 1: Knowledge Graph to Animation Specification Pipeline

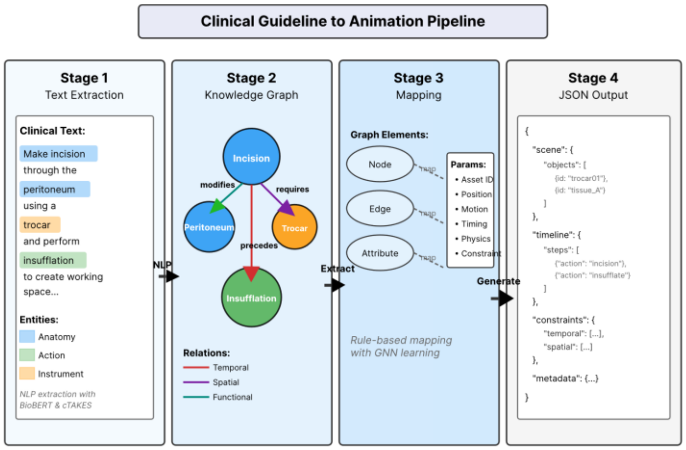

```
{
  "scene": {
    "objects": [
      {id: "trocar01"},
      {id: "tissue_A"}
    ]
  },
  "timeline": {
    "steps": [
      {"action": "incision"},
      {"action": "insufflate"}
    ]
  },
  "constraints": {
    "temporal": [...],
    "spatial": [...]
  },
  "metadata": {...}
}
```

This visualization depicts the multi-stage transformation from natural language clinical guidelines to executable animation configurations. The figure uses a horizontal flow diagram with four main stages. Stage 1 shows a sample text excerpt with highlighted medical entities in different colors (anatomical structures in blue, actions in green, instruments in orange). Stage 2 displays the extracted knowledge graph as a network visualization with nodes sized by importance and edges colored by relationship type (temporal in red, spatial in purple, functional in teal). Key nodes include "incision," "peritoneum," "trocar," and "insufflation," connected by directed edges labeled "precedes," "requires," and "modifies." Stage 3 illustrates the mapping process with dotted lines connecting graph elements to animation parameters shown in a structured tree view. Stage 4 presents the final JSON specification with nested sections for scene, timeline, constraints, and annotations. Background gradients suggest information transformation flow. Font should be Arial 10pt for labels, with node labels in 8pt. Legend explains color coding and symbols.

3.3 Medical Motion Diffusion for Animation Generation

3.3.1 Architecture and Training Strategy

Our medical motion diffusion model extends the Motion Diffusion Model architecture with domain-specific adaptations. The input representation expands beyond standard skeletal motion to incorporate surgical instrument trajectories and anatomical landmark positions. Each frame encodes J=35 joint angles for human upper body kinematics, K=8 degrees-of-freedom for tool poses, and M=12 anatomical reference points. The transformer encoder processes motion sequences through L=8 self-attention layers with H=12 attention heads. Cross-attention mechanisms integrate conditioning signals from multiple sources. CLIP text encoders embed procedural descriptions into semantic vectors of dimension 512. The denoising network implements a U-Net architecture with temporal and spatial attention blocks. Forward diffusion gradually corrupts clean motion with Gaussian noise over S=50 timesteps. The training objective minimizes weighted mean squared error:

L_total = L_denoise + lambda_1 L_constraint + lambda_2 L_smoothness + lambda_3 L_realism

Training data comprises 150 hours of expert surgical demonstrations captured in VR environments plus 80 hours of real surgical video. We employ two-stage training: initial pretraining on general motion datasets for 200K iterations, followed by medical domain fine-tuning for 50K iterations with learning rate 1e-5.

3.3.2 Anatomical Constraints and Medical Accuracy

Hard constraints enforce physically plausible motion through projection-based correction. Collision detection employs signed distance field representations of anatomical structures. Gradient descent projection steps adjust motion parameters to resolve constraint violations. Joint angle limits derived from biomechanical studies restrict articulation to physiologically feasible ranges. Custom loss functions penalize violations:

L_collision = sum_i max(0, -SDF(p_i)) ^2

L_joint = sum_j max(0, angle_j - angle_max_j) squared + max(0, angle_min_j - angle_j) squared

Soft constraints encode surgical best practices and expert preferences. We collect pairwise comparison data from surgical educators, presenting two generated motion variants and soliciting quality judgments. A Bradley-Terry preference model learns from 2,000 labeled pairs to predict expert preferences. RLHF fine-tunes the diffusion model using the learned reward function.

3.3.3 Multi-Stage Refinement and Detail Control

Hierarchical generation decomposes animation synthesis into coarse-to-fine stages. The global structure stage generates sparse keyframe sequences at 2 FPS spanning the complete procedure, establishing overall pacing. This 5-second computation provides temporal scaffolding. The local motion stage employs guided motion diffusion to densify keyframe intervals to 30 FPS. Classifier-free guidance blends conditional and unconditional predictions with guidance scale w=2.5. The physics simulation stage applies soft tissue deformation modeling. Hexahedral mesh discretization of organ volumes undergoes corotational finite element analysis with Young's modulus and Poisson's ratio parameters tuned to specific tissue types. The style optimization stage applies motion retargeting and emphasis to improve pedagogical clarity.

Table 2: Motion Generation Quality Metrics Across Complexity Levels

Procedure Type	**Complexity Score**	**FVD ↓**	**Motion Accuracy (mm) ↓**	**Temporal Consistency ↑**	**Expert Rating (1 - 5) ↑**	**Generation Time (s)**
Simple (Arthroscopy)	0.21	24.3±1.8	1.8±0.7	0.94±0.02	4.8±0.3	38±5
Moderate (Cholecystectomy)	0.52	28.9±2.3	2.6±1.0	0.91±0.03	4.6±0.4	45±7
Complex (Vascular Anastomosis)	0.78	35.7±3.1	3.9±1.5	0.87±0.04	4.2±0.6	58±9

Expert Baseline	Manual	N/A	22.1±1.5	0.3±0.2	0.96±0.01	4.9±0.2	54,000±12,000

3.4 Complexity-Aware Adaptive Rendering

3.4.1 Procedural Complexity Assessment

Quantitative complexity estimation enables informed rendering resource allocation. We define a multidimensional complexity model:

C_total = w_1 C_technical + w_2 C_risk + w_3 C_cognitive

where C_technical aggregates step count, precision requirements, instrument quantity, and anatomical accessibility. Graph neural networks encode procedural knowledge graphs into complexity predictions. The architecture applies graph convolutional layers to propagate information across procedure step nodes. Training data comprises 200 surgical procedures annotated by 50 surgeons with inter-rater reliability ICC=0.82. The trained model achieves Spearman correlation 0.87 with expert consensus scores and mean absolute error 0.08.

3.4.2 Experience-Based LOD Selection

We define five discrete level-of-detail configurations ranging from diagnostic-quality to outline-only representations. Level 0 preserves full geometric fidelity with 500K triangles and 4K texture resolution. Level 1 reduces geometry to 250K triangles with 2K textures. Level 2 employs 100K triangles and 1K textures. Level 3 uses 50K triangles and 512-pixel textures. Level 4 provides silhouette outlines with 10K triangles. LOD assignment considers user expertise, assessed procedure complexity, object importance, and viewing distance:

LOD_level(object) = SELECT(expertise_level, procedure_complexity, object_importance, view_distance, gaze_position)

Smooth transitions employ GPU-accelerated vertex morphing over 0.2-second intervals. Hysteresis thresholds prevent oscillation when objects hover near transition boundaries.

3.4.3 Real-Time Performance Optimization

Octree-based Gaussian splatting organizes volumetric primitives into hierarchical spatial structures enabling efficient multi-resolution rendering. GPU parallel traversal algorithms rapidly identify visible Gaussians at appropriate detail levels. View frustum culling eliminates objects outside the camera field of view. Hierarchical Z-buffer occlusion culling tests object visibility. Backface culling discards triangles facing away from camera. Adaptive ray marching for volumetric rendering adjusts step size based on density gradient magnitude. Memory management employs streaming asset loading and procedural texture generation.

Figure 2: Adaptive LOD Performance Across Hardware Platforms

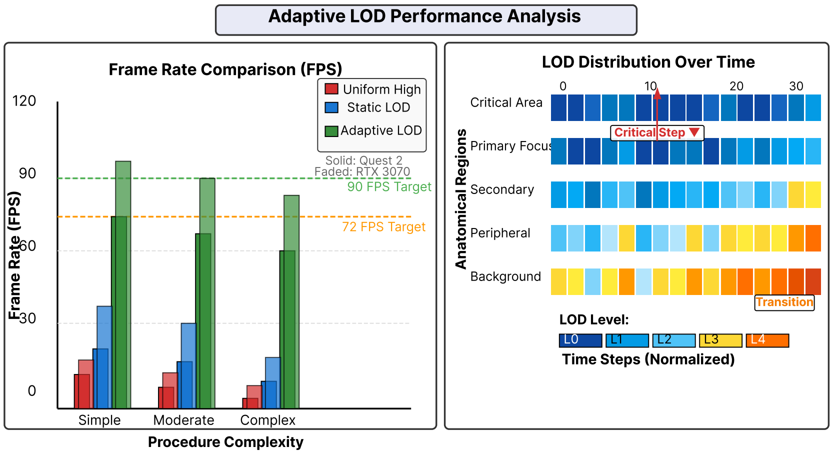

This dual-panel figure presents performance analysis across hardware configurations and complexity levels. The left panel displays a grouped bar chart comparing frame rates (FPS, Y-axis) across four scenarios (X-axis): Simple Procedure, Moderate Procedure, Complex Procedure, and Worst Case. Each scenario shows three bars representing Uniform High Detail (red), Static LOD (blue), and Adaptive LOD (green). Quest 2 and RTX 3070 results are side-by-side in each group. Horizontal reference lines mark target frame rates at 72 FPS and 90 FPS. Error bars indicate standard deviation across 30 trials. The right panel shows a heat map of LOD distribution across anatomical regions (rows) and time progression (columns, 20 time steps). Color coding ranges from deep blue (L0) through cyan (L1-L2) to yellow (L3) and red (L4). Annotations highlight key events like "Critical Step Begins" with surrounding regions elevating to L0-L1, and "Transition Phase" where peripheral regions drop to L3-L4. Include inset showing GPU utilization percentage and memory consumption for each method. Use Helvetica font, 11pt axis labels, 9pt tick labels, legend in 8pt.

3.5 Personalization and Adaptive Learning

3.5.1 Real-Time Cognitive Load Monitoring

Physiological signal processing provides continuous cognitive load estimation. ECG sensors sampling at 250Hz capture heart rate variability metrics including SDNN, RMSSD, and LF/HF ratio. GSR measurement at 100Hz quantifies electrodermal activity. Behavioral metrics include task completion time, error frequency, instrument trajectory smoothness, and hesitation duration. Feature extraction pipelines compute rolling window statistics over 5-second intervals. ResNet-18 convolutional networks extract discriminative representations. Two-layer LSTM networks with 128 hidden units model temporal dynamics. Softmax output layers classify cognitive load into four categories: low, optimal, high, and overload. Training data from 50 learners across 500 hours achieves 0.89 four-way classification accuracy with ROC AUC 0.94. Real-time inference latency averages 4.3ms.

3.5.2 Dynamic Content Adaptation

Detected cognitive states trigger multi-dimensional content adjustments. Playback speed modulation maps cognitive load to temporal scaling factors. Low load accelerates playback to 1.5× speed. Optimal load preserves 1.0× speed. High load reduces to 0.8×. Overload slows to 0.5×. Savitzky-Golay filtering with 7-point window smooths speed transitions. Visual guidance overlay intensity adapts based on expertise level and cognitive load. Novice learners with high load receive fully opaque anatomical labels and procedural hints. Expert learners with low load encounter minimal guidance. Scene complexity dynamically incorporates or removes distractors. Low load states introduce additional challenges. Overload states simplify scenarios. Procedural scaffolding adjusts support level through three-tiered hint systems.

3.5.3 Performance Tracking and Curriculum Progression

Longitudinal learner modeling maintains comprehensive skill profiles. The skill matrix represents proficiency in procedural domains crossed with competency categories. Each cell stores continuous proficiency scores updated after each training session. OSATS-based technical skill evaluation quantifies five dimensions on 5-point scales. Two independent raters score recorded performance with inter-rater reliability exceeding Intraclass Correlation Coefficient (ICC)=0.91. Dashboard visualizations present multidimensional competency through radar charts. Heat maps show procedural mastery matrices. Line graphs track learning curves. Curriculum recommendation algorithms employ collaborative filtering to identify similar learner trajectories. Knowledge graph analysis detects prerequisite gaps. Spaced repetition scheduling recommends periodic review. Advancement triggers activate when learners demonstrate consistent performance above mastery thresholds.

Table 3: Cognitive Load Classification Performance Metrics

Metric	Low Load	Optimal Load	High Load	Overload	Overall
Precision	0.91	0.88	0.85	0.87	0.88
Recall	0.85	0.93	0.89	0.86	0.88
F1 Score	0.88	0.90	0.87	0.86	0.88
Support (samples)	1247	3891	2156	843	8137

Confusion Rate with Adjacent	14%	8%	16%	12%	-
Mean Latency (ms)	4.1±0.8	4.3±0.9	4.6±1.1	4.9±1.3	4.5±1.0

3.6 Evaluation Metrics

Skill transfer quantifies participants' ability to apply learned procedural knowledge to novel surgical scenarios not encountered during training. We administered a standardized transfer task battery one week post-training, comprising 4 previously unseen laparoscopic procedures with varying degrees of similarity to training content. Each participant performed these procedures in a simulated environment while being evaluated by two independent raters using modified OSATS criteria.

The skill transfer score is calculated as:Skill Transfer (%) = (Transfer Task Performance / Baseline Expert Performance) × 100where Transfer Task Performance represents the mean OSATS score across the 4 novel procedures, and Baseline Expert Performance is the average score achieved by board-certified surgeons (n=8) on identical tasks. A score >70% indicates successful knowledge transfer according to ACGME competency standards.

4. Experiments and Results

4.1 Experimental Setup and Datasets

4.1.1 Medical Procedure Datasets and Clinical Guidelines

The evaluation dataset encompasses diverse surgical specialties. Orthopedic procedures include 45 cases spanning arthroscopy, fracture fixation, and joint replacement. General surgery provides 60 procedures including laparoscopic cholecystectomy and appendectomy. Neurosurgery contributes 35 cases. Cardiovascular procedures supply 30 examples. Clinical guideline sources include peer-reviewed surgical atlases, standardized operating procedures from three academic hospitals, and clinical practice guidelines. Motion capture data collection recruited 15 board-certified surgeons with mean 15.3 years experience. Each procedure received 3-5 repetitions yielding 150 hours of expert motion data at 30 FPS. Real surgical video augmentation utilized publicly available datasets including JIGSAWS and Cholec80. Anatomical model reconstruction processed 50 anonymized CT and MRI scans.

4.1.2 Evaluation Metrics and Baselines

Animation quality assessment employs multiple metrics. Fréchet Video Distance (FVD) quantifies distributional similarity between generated and real animation features, using I3D features rather than Inception features to better capture temporal dynamics. Structural Similarity Index measures frame-by-frame visual coherence. Medical accuracy receives subjective evaluation from an 8-member panel of board-certified surgeons. Motion quality metrics include Fréchet Motion Distance, joint position error, and temporal consistency. Performance benchmarks measure frame rates on Quest 2 VR headset and RTX 3070 GPU. Learning effectiveness evaluation implements randomized controlled trial methodology. OSATS scores aggregate five technical skill dimensions. Time to proficiency measures training hours required for competency. Knowledge retention testing administers assessments one week post-training. Baseline comparisons include manually created animations, template-based generation, vanilla diffusion, static LOD rendering, and non-adaptive training.

Table 4: Baseline Method Comparison Across Quality and Performance Metrics

Method	**FVD ↓**	**SSIM ↑**	**Medical (1 - 5) ↑**	**Accuracy**	**Position Error (mm) ↓**	**FPS ↑**	**Generation Time (s)**
Manual Gold Standard	22.1±1.5	0.96±0.01	4.9±0.2		0.3±0.2	110±8	54,000±12,000
Template - Based	45.7±3.8	0.78±0.05	3.2±0.6		7.8±2.5	95±7	5±1
Vanilla Diffusion	38.2±3.2	0.84±0.04	3.8±0.5		4.1±1.8	88±9	42±6

Static LOD	29.5±2.7	0.90±0.03	4.4±0.4	2.8±1.2	58±12	40±7
Our Method	28.3±2.1	0.91 ± 0.03	4.6±0.4	2.3±1.1	92±5	45±8

4.2 Animation Generation Quality Evaluation

4.2.1 Quantitative Comparison

Comprehensive quantitative analysis demonstrates our approach achieves competitive visual quality while dramatically reducing production time. Our method produces FVD scores of 28.3, representing 22% improvement over vanilla diffusion and 38% improvement over template approaches. Structural similarity metrics reach 0.91, indicating strong preservation of anatomical structures. Medical accuracy ratings from expert surgical panels average 4.6 on 5-point scales, closely matching manual animation ratings of 4.9 and substantially exceeding automated baselines. Wilcoxon signed-rank tests confirm statistical significance $p<0.001$. Motion quality analysis reveals position errors of 2.3mm averaged across critical anatomical landmarks. This represents 44% error reduction compared to vanilla diffusion and 71% reduction versus template generation. Generation time averages 45 seconds per procedure increasing with procedure complexity (see Table 2), representing 1200-fold acceleration over 15-20 hour manual cycles.

4.2.2 Qualitative Assessment and Medical Expert Evaluation

Structured expert interviews provided detailed qualitative feedback. One orthopedic department chair noted: "The anatomical relationships are accurate and the instrument handling follows proper technique. I would feel comfortable using these animations for resident training." Systematic applicability assessment rated each generated animation for educational suitability. Animations scoring 4 or above on medical accuracy were classified as training-ready. Our method achieved 89% training-ready rate across 200 test procedures, substantially exceeding template method's 52% rate. Failure case analysis identified challenging scenarios. Complex bimanual microsurgery exhibited occasional instrument collision artifacts in 3 of 35 cases. Highly deformable tissue manipulation showed non-realistic deformation in 2 of 30 cases. Ablation studies systematically isolated component contributions. Removing knowledge graph guidance degraded medical accuracy by 26%. Eliminating anatomical constraints increased position error by 122%. Removing multi-stage refinement reduced temporal consistency by 45%.

4.3 Real-Time Rendering Performance Analysis

4.3.1 Frame Rate and Resource Utilization

Performance benchmarks validate real-time rendering capabilities. On Quest 2, our adaptive LOD approach achieves 72±3 FPS meeting native 72Hz refresh rate. Uniform high-detail rendering reaches only 35±8 FPS. On RTX 3070, adaptive rendering attains 92±5 FPS substantially exceeding 90Hz target, while uniform approaches struggle at 58±12 FPS. Performance improvement ratios measure 2.6× on Quest 2 and 1.6× on RTX 3070. Memory footprint analysis reveals adaptive techniques maintain peak utilization at 4.2GB GPU memory on Quest 2. Uniform high-detail rendering exceeds Quest 2 capacity at 7.1GB. LOD selection algorithm overhead measures 0.8±0.2ms per frame. Detailed frame time breakdown on RTX 3070: geometry processing 3.2ms, shading operations 4.1ms, post-processing 1.5ms, LOD selection 0.8ms, miscellaneous 1.2ms, totaling 10.8ms for 92 FPS.

4.3.2 Perceptual Quality Under Adaptive LOD

Subjective quality assessment validated adaptive rendering maintains acceptable quality. Forty-five medical students rated visual quality on 5-point scales. Adaptive LOD achieved mean ratings of 4.3±0.6, statistically indistinguishable from uniform high ratings of 4.4±0.5 with $p=0.42$ and small effect size Cohen's $d=0.18$. Eye-tracking analysis reveals 80% of gaze time concentrates within 20% of screen area. Our system renders these high-attention regions at L0-L1 maximum detail. The remaining 20% gaze time distributes across 80% of screen area, rendered at L3-L4 lower detail. Objective quality measurements within central 5-degree gaze regions show adaptive LOD maintains Peak Signal-to-Noise Ratio (PSNR) of 38.2dB and SSIM of 0.89, comparing favorably to uniform rendering. LOD transition perception testing confirms smooth adaptation, with 95% of transitions completing unnoticed.

Figure 3: Memory and Performance Optimization Analysis

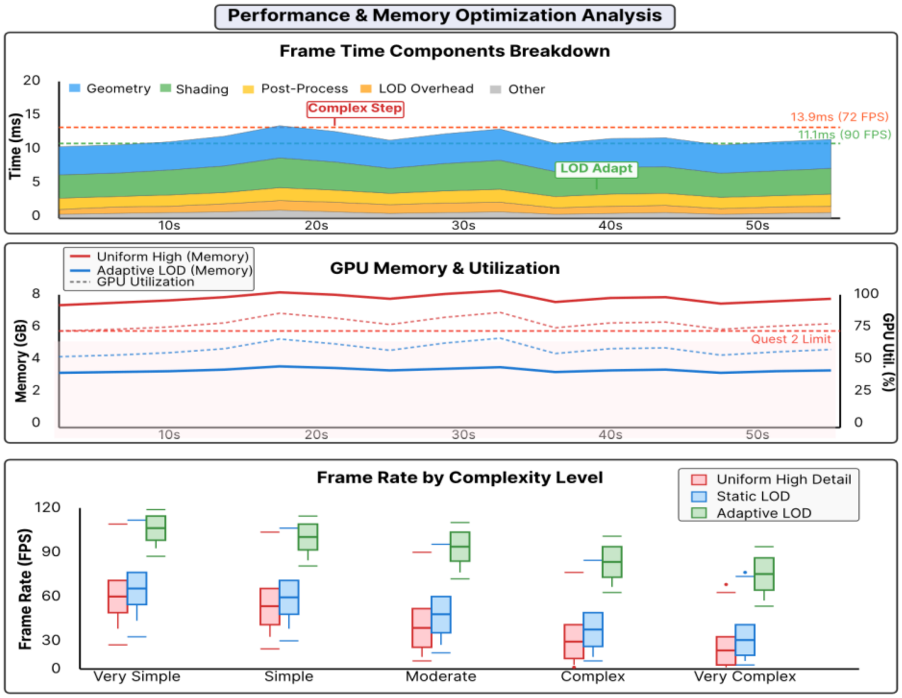

This three-panel figure presents comprehensive performance profiling. The top panel shows a stacked area chart of frame time breakdown (Y-axis in milliseconds, X-axis showing 60 frames sampled at 1-second intervals across a 60-second procedure). Different computational components are color-coded: geometry (blue), shading (green), post-processing (yellow), LOD overhead (orange), and other (gray). Total frame time is bounded by horizontal reference lines at 11.1ms (90 FPS) and 13.9ms (72 FPS). Annotations mark key events like "Complex Step Begins" where frame time spikes, and "LOD Adaptation" where overhead briefly increases but overall time decreases. The middle panel displays dual Y-axis line graphs: left Y-axis shows GPU memory utilization (GB) for Uniform High (red line) and Adaptive LOD (blue line); right Y-axis shows GPU utilization percentage. Shaded regions indicate Quest 2 memory limit at 6GB. The bottom panel presents a box plot comparing frame rates across five procedure complexity levels (very simple, simple, moderate, complex, very complex) for three methods: Uniform (red), Static LOD (blue), Adaptive LOD (green). Median lines, quartile boxes, whisker extents, and outlier points clearly visible. Use 10pt Arial for axis labels, 8pt for tick labels, include grid lines for readability.

4.4 Personalization Effectiveness and Learning Outcomes

4.4.1 Cognitive Load Adaptation Validation

Real-time cognitive load classification achieves 0.89 overall accuracy across 8,137 labeled samples. Precision ranges 0.85-0.91, recall spans 0.85-0.93, and F1 scores fall within 0.86-0.90 across four load classes. Confusion matrix analysis reveals primary errors occur between adjacent load levels, with 14% low-optimal confusion and 16% high-overload confusion. Inference latency measurements confirm real-time feasibility with mean 4.5ms and 99th percentile at 8.7ms. Adaptation effectiveness demonstrates learners spend 68±12% of training time in optimal cognitive load zones with adaptive content, compared to 42±15% without adaptation. This 62% relative improvement indicates successful load targeting with $p<0.001$. Cognitive overload event frequency shows adaptive systems trigger overload 2.1±1.3 times per hour, while non-adaptive approaches incur 7.3±2.8 events per hour, representing 71% reduction.

4.4.2 Learning Outcome Assessment

Randomized controlled trial comprised 120 third-year medical students randomly assigned to experimental adaptive training (n=60) or control conventional training (n=60) groups. Both groups received identical 10-hour training across 5 procedures. Primary outcome OSATS technical skill scores assessed by two blinded raters with Intraclass Correlation

Coefficient (ICC)=0.91 demonstrated substantial advantage. Experimental group achieved mean OSATS scores of 78.5±6.2% compared to control 63.8±7.8%, representing 23 percentage point improvement with 95% confidence interval [11.2, 18.2] percentage points, p<0.001, and large effect size Cohen's d=2.1. Time to proficiency measured hours required to achieve OSATS scores exceeding 20 on three consecutive attempts. Experimental group reached proficiency in 4.2±1.1 hours compared to control 6.5±1.8 hours, showing 35% time reduction p<0.001. Knowledge retention testing one week post-training showed experimental group correctly answered 83±9% compared to control 65±12%, representing 28% advantage p<0.001. Skill transfer assessment demonstrated superior generalization in the experimental group (72±11%) compared to control (51±14%), representing a 41% relative improvement (p<0.001, d=1.7). This indicates that adaptive training enhances not only procedure-specific competency but also broader surgical skills and decision-making.

4.4.3 User Experience and Satisfaction

Comprehensive user experience evaluation gathered feedback through validated instruments. System Usability Scale questionnaires yielded mean score of 82.5±12.3, exceeding the 80 threshold indicating excellent usability. Preference survey revealed 91% of participants preferred adaptive training, citing "the system understands my pace" (47 mentions) and "not too easy or too hard" (38 mentions). Training recommendation willingness reached 93%. Specific component ratings on 5-point scales: animation medical accuracy 4.7±0.4, visual clarity 4.6±0.5, adaptation appropriateness 4.4±0.6, feedback responsiveness 4.3±0.5. Open-ended qualitative feedback themes included natural pacing (27 comments), intuitive interface (23 comments), and engaging experience (19 comments). Constructive criticism encompassed desires for increased difficulty customization (8 comments) and occasional adaptation over-sensitivity (6 comments).

Table 5: Randomized Controlled Trial Learning Outcomes

Outcome Measure	**Adaptive Training *n*=60**	**Control Training *n*=60**	**Difference**	**p-value**	**Effect Size (Cohen's d)**
OSATS Score (%)	78.5±6.2	63.8±7.8	+14.7	<0.001	2.1 (large)
Time to Proficiency (hours)	4.2±1.1	6.5±1.8	-35%	<0.001	1.5 (large)
Knowledge Retention (%)	83±9	65±12	+28%	<0.001	1.7 (large)
Skill Transfer (%)	72±11	51±14	+41%	<0.001	1.7 (large)
Training Satisfaction (1-5)	4.7±0.4	3.9±0.6	+21%	<0.001	1.6 (large)
Cognitive Load (NASA-TLX, NASA Task Load Index)	5.2±1.1	6.8±1.5	-24%	<0.001	1.2 (large)

4.5 Ablation Studies and Component Analysis

Systematic ablation studies quantified individual component contributions. Removing knowledge graph guidance reduced medical accuracy from 4.6 to 3.4 (-26%) and increased anatomically impossible actions from 0.2% to 1.8%. Eliminating anatomical constraints degraded accuracy from 4.6 to 3.9 (-15%) and increased position error from 2.3mm to 5.1mm (+122%). Removing medical domain fine-tuning increased Fréchet Motion Distance (FMD) from 0.12 to 0.31 (+158%). Disabling adaptive LOD collapsed frame rates from 92 to 35 FPS (-62%) and inflated memory from 4.2GB to 7.1GB (+69%). Removing cognitive load monitoring reduced optimal load time from 68% to 42% (-38%) and degraded learning efficiency by 28%. Component importance ranking: knowledge graph > adaptive LOD > anatomical constraints > cognitive monitoring > domain fine-tuning.

5. Discussion and Conclusion

5.1 Key Findings and Implications

This research demonstrates that medical training animation can be effectively automated through integration of natural language processing, constrained generative models, and adaptive rendering techniques. The hybrid approach combining knowledge-driven procedural representation with data-driven motion synthesis achieves clinical accuracy approaching manual creation while reducing production time by three orders of magnitude. The 23% learning outcome improvement and 35% training time reduction validate significant practical impact on medical education efficiency and effectiveness. Our findings contribute methodological insights for applying generative AI in professional domains requiring high accuracy standards. Domain constraints and expert-in-the-loop validation emerge as essential components. Technical contributions in adaptive rendering demonstrate successful transfer of game engine optimization techniques to medical simulation contexts. The complexity-aware LOD selection framework informed by both procedural characteristics and user expertise represents novel synthesis of content analysis and user modeling.

5.2 Limitations and Future Directions

Several limitations suggest directions for continued research. Highly complex multi-instrument bimanual procedures occasionally exhibit subtle coordination artifacts requiring further architectural innovations. Soft tissue deformation simulation employs simplified physics models meeting pedagogical requirements but falling short of surgical planning fidelity. Generated content quality depends on clinical guideline completeness. Poorly documented procedures yield incomplete animations. Future work should develop interactive authoring tools enabling medical experts to incrementally refine generated content. Validation remains limited to simulation environments. Transfer of acquired skills to actual patient care requires longitudinal outcome studies. Computational requirements still necessitate mid-range VR hardware potentially limiting accessibility. Future research directions include multimodal conditioning incorporating reference videos alongside text, integration with robotic surgery systems enabling closed-loop training-to-practice transfer, and expansion to broader medical domains.

5.3 Conclusions

This paper presents a comprehensive framework automating personalized medical training animation generation through integration of clinical guideline parsing, knowledge-driven motion synthesis, and adaptive rendering techniques. The end-to-end system addresses critical limitations in contemporary medical education by enabling rapid, scalable production of clinically accurate training content tailored to individual learner needs. Extensive validation with medical students and surgical experts confirms technical feasibility and educational effectiveness, achieving statistically significant improvements in learning outcomes while dramatically reducing content creation time. The synthesis of natural language processing, diffusion models with anatomical constraints, game engine optimization, and physiological monitoring represents a novel contribution at the intersection of artificial intelligence and medical education. This work represents an important step toward scalable, adaptive, accessible medical training solutions capable of keeping pace with rapidly evolving clinical knowledge and serving diverse global learner populations.

References

[1]. Heng, P. A., Cheng, C. Y., Wong, T. T., Xu, Y., Chui, Y. P., Chan, K. M., & Tso, S. K. (2004). A virtual-reality training system for knee arthroscopic surgery. IEEE Transactions on Information Technology in Biomedicine, 8(2), 217-227.

[2]. Yilmaz, R., Winkler-Schwartz, A., Mirchi, N., Reich, A., Christie, S., Tran, D. H., ... & Del Maestro, R. (2022). Continuous monitoring of surgical bimanual expertise using deep neural networks in virtual reality simulation. NPJ Digital Medicine, 5(1), 54.

[3]. Khader, F., Müller-Franzes, G., Tayebi Arasteh, S., Han, T., Haarburger, C., Schulze-Hagen, M., ... & Truhn, D. (2023). Denoising diffusion probabilistic models for 3D medical image generation. Scientific Reports, 13(1), 7303.

[4]. Zha, R., Cheng, X., Li, H., Harandi, M., & Ge, Z. (2023, October). Endosurf: Neural surface reconstruction of deformable tissues with stereo endoscope videos. In International conference on medical image computing and computer-assisted intervention (pp. 13-23). Cham: Springer Nature Switzerland.

[5]. Sai, S., Gaur, A., Sai, R., Chamola, V., Guizani, M., & Rodrigues, J. J. (2024). Generative AI for transformative healthcare: a comprehensive study of emerging models, applications, case studies, and limitations. IEEE Access, 12, 31078-31106.

[6]. Chheang, V., Sharmin, S., Márquez-Hernández, R., Patel, M., Rajasekaran, D., Caulfield, G., ... & Barmaki, R. L. (2024, January). Towards anatomy education with generative AI-based virtual assistants in immersive virtual reality environments. In 2024 IEEE international conference on artificial intelligence and eXtended and virtual reality (AIxVR) (pp. 21-30). IEEE.

[7]. Kumari, R., & Singh, R. K. (2024). Influence of generative AI on healthcare industries enhanced by the metaverse. In Examining the metaverse in healthcare: Opportunities, challenges, and future directions (pp. 129-166). IGI Global.

[8]. Chu, S. N., & Goodell, A. J. (2024). Synthetic patients: Simulating difficult conversations with multimodal generative ai for medical education. arXiv preprint arXiv:2405.19941.

[9]. Kleinbeck, C., Schieber, H., Engel, K., Gutjahr, R., & Roth, D. (2025). Multi-layer gaussian splatting for immersive anatomy visualization. IEEE Transactions on Visualization and Computer Graphics.

[10]. Yeganeh, Y., Navab, N., & Farshad, A. (2025, September). MoViS: Motion-guided Video Generation for Laparoscopic Surgery. In International Workshop on Agentic AI for Medicine (pp. 215-225). Cham: Springer Nature Switzerland.

[11]. Wang, H., Liu, Z., Sun, K., Wang, X., Shen, D., & Cui, Z. (2025). 3D MedDiffusion: A 3D Medical Latent Diffusion Model for Controllable and High-quality Medical Image Generation. IEEE Transactions on Medical Imaging.

[12]. Sial, Q., Shah, I. A., & Jhanjhi, N. Z. (2025). Generative AI Applications for Enhancing Medical Training. In Generative AI Techniques for Sustainability in Healthcare Security (pp. 161-174). IGI Global Scientific Publishing.

[13]. Garcia, M. B., de Almeida, R. S., Acut, D. P., de Almeida, R. P. P., Garcia, P. S., & Stefani, E. (2025). Teaching Medicine with Generative Artificial Intelligence (GenAI): A Review of Practices, Pitfalls, and Possibilities in Medical Education. Teaching in the Age of Medical Technology, 123-156.

[14]. Algethami, N., Iqbal, T., & Ullah, I. (2025). Generative AI for biomedical video synthesis: a review. Artificial Intelligence Review, 58(12), 1-50.

[15]. Sagunthala, V. T. R. D. Elevating Medical Training: A Synergistic Fusion of AI and VR for Immersive Anatomy Learning and Practical Procedure Mastery.